

Determination of the intrinsic velocity field in the M87 jet

Chun-Cheng Wang^{1,2*} and Hong-Yan Zhou^{1,2}

¹Center for Astrophysics, University of Science and Technology of China, Hefei, Anhui 230026, P.R. China

²Joint Institute for Galaxy and Cosmology (JOINGC), SHAO and USTC, CAS

Accepted 2008 December 30. Received 2008 December 2; in original form 2007 December 4

ABSTRACT

A new method to estimate the Doppler beaming factor of relativistic large-scale jet regions is presented. It is based on multiwaveband fitting to radio-to-X-ray continua with synchrotron spectrum models. Combining our method with available observational data of proper motions, we derive the intrinsic velocity as well as the viewing angles to the line of sight for eight knotty regions down the M87 jet. The results favor the ‘modest beaming’ scenario along the jet, with Doppler factors varying between $\sim 2-5$. The inner jet of M87 suffers sharp deceleration, and the intrinsic speed remains roughly constant down the outer jet. The orientation of the inner jet regions is fully consistent with the result of $10^\circ-19^\circ$ to the line of sight suggested by previous *Hubble Space Telescope* (HST) proper motion studies of the M87 jet. The outer jet, however, shows systematic deflection off the inner jet to much smaller inclination ($\theta \ll 10^\circ$). Further calculation of knot A suggests this deflection can be regarded as evidence that the outer jet suffers some departure from equipartition. The nucleus region of the M87 jet should have a viewing angle close to its first knot HST-1, i.e. $\theta \sim 15^\circ$, which favors the idea that M87 may be a misaligned blazar. This work provides some hints about the overall dynamics of this famous extragalactic jet.

Key words: galaxies: active – galaxies: individual (M87) – galaxies: kinematics and dynamics – galaxies: jets.

1 INTRODUCTION

Since the discovery of the first extragalactic large-scale jet in a nearby active galaxy M 87 (Curtis 1918), intense efforts are made to explore the underlying physics of the relativistic jets during the past decades. The related topics concern about the matter content, particle acceleration, collimation mechanism and magnetic field configuration inside the jet flow. Among these problems, one of the fundamental issues is the intrinsic velocity field of the jet. Lack of an effective method to determine the speed and orientation of the successive regions in large-scale jet, it is difficult to constrain further the mechanism on overall dynamics of the bulk jet flow.

In this work, a new method is presented to estimate the Doppler beaming factor in a region of large-scale jet. This method is based on the spectral fit of the multi-waveband continua with standard synchrotron radiation models. Combining the data of proper motions, we readily derive the intrinsic bulk velocity as well as the angle to line-of-sight of the jet flow. Making application of this new method, we successfully obtain the intrinsic velocity field in M 87 jet.

Our result agrees well with that of the new variability monitoring program toward the same object (Harris et al. 2006), which indicates the reliability of our approach. The method is simple and only requires non-simultaneous spectral energy distribution (SED) data sets, therefore is hopeful to be of general interest for those synchrotron-dominated jets.

For the rest of this paper, we firstly make synchrotron spectrum model fitting to radio-to-X-ray SED of M87 jet in §2, then introduce the new method and derive the distribution of Doppler beaming factor along M 87 jet in §3. Coupling the data of proper motions, we obtain the intrinsic velocity field of M87 jet in §4. Related discussions are also presented in this section. Finally, the main results are summarized in §5.

2 SYNCHROTRON SPECTRUM MODEL FITTING TO M87 JET

2.1 The Synchrotron Radiation Models

The high spatial resolution of *Chandra* X-ray observatory (FWHM = $0.5''$) has opened a new era on the research of extragalactic large-scale jets at high energy waveband. At the time of preparing this paper, 91 radio-loud AGNs are re-

* E-mail: ccwang@ustc.edu.cn

ported detection of X-ray counterparts of radio jets on large-scales (see also <http://hea-www.harvard.edu/XJET/>). The number of detected X-ray jets increases rapidly, suggesting that X-ray emission from jets is a common feature in radio galaxies and quasars. If combined with observational data in radio and optical band (sometimes also with available infrared and ultraviolet data), we can construct broadband SED and carry out multi-waveband modelling of the jet regions. Such a procedure may provide us with useful information of jet physics.

Polarization observations already confirm the synchrotron nature of the radio-optical emissions from extragalactic jets (e.g., Perlmutter et al. 1999 for M 87 jet). The X-ray emission process of large-scale jets, however, remains as an open question. For nearby FR I radio galaxies, the radio-to-X-ray SED from the large-scale knots is consistent with a single smoothly broken power-law spectrum, and the expected inverse-Compton scattering (IC) fluxes of seed photons (jet synchrotron photons or cosmic microwave background photons) always underpredict the observed X-ray fluxes. This implies the synchrotron origin of the X-ray emissions observed in FR I jets (e.g., Marshall et al. 2002 and Wilson & Yang 2002 for M 87, Hardcastle, Birkinshaw & Worrall 2001 for 3C 66B). The recent statistical research of a large X-ray jet sample (Kataoka & Stawarz 2005) also favors this physical picture. On the other hand, the X-ray emissions from large-scale quasar and FR II jets, however, are usually interpreted as inverse-Compton scattering of CMB photons within a highly relativistic jet (Harris & Krawczynski 2002).

As discussed by Schwartz (2002), the IC/CMB model for the X-ray emissions of large-scale quasar jets predicts two main differences between nearby and distant objects. Due to the enhancement of the CMB energy density with redshift by a factor of $(1+z)^4$, the ratio of X-ray to radio fluxes of the resolved parts of the quasar jets should increase in distant sources compared to nearby ones. The other effect is that we should observe some systematic flattening of the optical-to-X-ray spectral index (α_{OX}) in distant unresolved quasar cores compared to low-redshift quasars, because of the increasing contribution from the unresolved portions of the jet to the X-ray flux of the quasar core.

We notice, however, the recent observational efforts of Lopez et al. (2006) to search the latter effect. They carry out a *Chandra* snapshot survey of representative high-redshift radio-loud quasars ($z \approx 3.5 - 4.7$) selected from the Parkes-MIT-NRAO sample. The survey does not detect any systematic flattening of the optical-to-X-ray spectral index (α_{OX}) of the unresolved quasar cores compared to low-redshift quasars. The results of Lopez et al. (2006) suggest that kiloparsec-scale X-ray emission of quasar jet is not dominated by inverse Compton scattering of CMB seed photons off jet electrons. Meanwhile, the IC/CMB model also meets difficulty in explaining the X-ray emissions from several FR II jets (e.g., Kraft et al. 2005 for 3C 403). It is also worthy to notice the most recent discovery of the X-ray counterjet in the FR II source 3C 353 detected by *Chandra* (Kataoka et al. 2008). The research of Kataoka et al. (2008) suggests that this detection is inconsistent with the IC/CMB model, and instead implies a synchrotron origin of the X-ray jet photons. Thus, even for powerful quasar/FR II jets, the

synchrotron radiation mechanism for X-ray photons keeps as a plausible interpretation.

In general, synchrotron origin for X-ray emission of large-scale jet faces much more strict challenge in particle acceleration than IC/CMB model does. Firstly, the particle acceleration in synchrotron X-ray jets has to be fast enough to generate ultra-relativistic electrons with maximum energies $\sim 10 - 100$ TeV (i.e., one to two orders of magnitude higher than that required in the IC/CMB model). Secondly, the electron acceleration processes in synchrotron X-ray jets have to operate continuously within the whole volumes of the jets. Such a strict requirement that synchrotron X-ray jets should work as powerful particle accelerators is naturally supported by the idea that large-scale jets are very hopeful sites for yielding Ultra High Energy Cosmic Ray particles (UHECRs, see e.g. Casse & Marcowith 2005 and references therein).

Based on the observations mentioned above, we choose synchrotron radiation model for our multi-waveband research. Currently, there are three standard synchrotron spectrum models available for statistical fit of SED: (1) The Jaffe & Perola (1973) model (hereafter JP), which assumes the pitch angle distribution of relativistic electrons is continuously isotropized after an initial injection of single power-law electron energy distribution. (2) The Kardashev-Pacholczyk model (Kardashev 1962 and Pacholczyk 1970, hereafter KP), which allows only the evolution of high energy tail of electron energy distribution following an initial single-power law electron injection. Since no pitch-angle scattering of the radiating electrons is allowed, it is unlikely to be the real case. This model, however, can give good fits to the observational data in many cases, therefore is relatively common in the jet research community. (3) The Continuous Injection model (Heavens & Meisenheimer 1987 and Meisenheimer et al. 1989, hereafter CI), which allows continuous electron injection with single power-law energy distribution into the emission region.

The spatial extent of the X-ray emitting regions in some FR I jets resolved by *Chandra* implies that continuous acceleration and injection of high-energy electrons may occur in these objects. On the other hand, recent work of Perlmutter & Wilson (2005) on M87 jet suggests that JP model underpredicts the X-ray flux by many orders of magnitude and the theoretical slope at X-ray energies is much larger than those observed. Therefore we do not consider the JP model in our work. All of the multi-band fits are made using KP and CI models. For all of the synchrotron spectrum models above, the dominated cooling process of high-energy electrons responsible for X-ray emissions should be synchrotron radiative energy loss.

2.2 Result of Multi-waveband Fit

M 87 is one of the nearby FR I radio galaxies (distance = 16 Mpc, with a scale of $1'' = 77.6$ pc). The rich observational data of its famous jet enable us to do further multi-band fit. The program of synchrotron spectrum fit we use is written by C. Carilli and J.P. Leahy (Carilli et al. 1991; Leahy 1991). The fit is done in two steps. In step 1, we get an initial guess of the position of the break frequency by employing a Myers and Spangler test (Myers & Spangler 1985) on the multi-waveband data sets. Then in step 2, a Marquardt non-linear

χ^2 test is done numerically (Press et al. 1987) to reach the best fitting of the SED data. The tests are model dependent. The electrons responsible for higher frequency synchrotron radiation suffer more rapid synchrotron loss, thus there is a spectra steepening toward the high frequency band. For CI model, there is a break in spectral index of $\Delta\alpha = 0.5$ between the low and high frequency spectra. In the case of KP model, $\Delta\alpha$ depends on the index of electron energy distribution.

In Figure 1, we plot results of CI as well as KP model fitting for the radio-to-X-ray SED of nucleus and eight knotty regions. It is worth to notice that knot HST-1 has started to flare (in radio, optical and X-ray waveband) around 2002 (Harris et al. 2006). Since we aim to do 'quiescent state fit' of the non-simultaneous SED, the broad-band data for this knotty region of M87 jet are carefully selected to be prior to the flare. The VLA observational data point at 15 GHz is from Zhou (1998), and optical-near-infrared data points are obtained with *HST* on 1998 (Perlman et al. 2001a). As to the X-ray spectrum, it is from Perlman & Wilson (2005), which is the reanalysis of early *Chandra* observations of M87 jet taken on 2000 July (Wilson & Yang 2002). The observations above locate prior to the outburst of HST-1 knot.

Moreover, Waters & Zepf (2005) present new ultraviolet *HST* observations of M87 jet taken on 2001 February 23. Their results suggest that knot HST-1 reveals a significant increase in the brightness from late 2001 to the present. Waters & Zepf (2005) try to do best fit to the observed radio-to-X-ray SED of HST-1 with standard synchrotron spectrum models, and found the new UV point exceeds the fit by a large amount independent of the models. Their work implies HST-1 knot has started its early evolution of the flare by the time of their observations. Therefore, we include the UV observational data points of Waters & Zepf (2005) for most M87 jet knots (no significant variability found up to date) except HST-1.

Table 1 lists the best-fit parameters for synchrotron spectrum models. During the fitting procedure, we set the input low frequency spectral index α_{inj} as the observed radio through optical spectral index α_{ro} (the same treatment as Perlman et al. 2001a). Here the convention of synchrotron spectrum is $S_\nu \propto \nu^{-\alpha}$.

In Figure 2, we plot the derived break frequency ν_{B} along M87 jet. Our result reveals a general trend of decline on the break frequency of large-scale knots, similar to that discovered by Marshall et al. (2002). We find, however, a significant increase of ν_{B} from jet nucleus to first knot, HST-1, by both of the model fitting. With CI model fitting to mid-IR SED, Perlman et al. (2001b) derived break frequency of M87 nucleus, $\nu_{\text{B}} = 2.8 \times 10^{12}$ Hz. The good agreement between our derived ν_{B} (2.22×10^{12} Hz) of the nucleus based on multi-waveband fitting and that of Perlman et al. (2001b) suggests that the increase-decline trend is reliable.

Here we discuss further the origin of broad-band spectra of the unresolved nucleus of M87 jet. There is some debate on this problem. Marshall et al. (2002) present high resolution X-ray image of M87 jet using *Chandra*. They find that the core flux is significantly larger than expected from an advection accretion flow and the spectrum is much steeper. Their results indicate that the X-ray emission of the M87 nucleus is due to synchrotron radiation from a small scale jet. Wilson & Yang (2002) also give *Chandra* X-ray imaging

and spectroscopy of M87 jet. In view of the similar spectra of the nucleus and jet knots, and the high X-ray flux of the knots closest to the nucleus, Wilson & Yang (2002) suggest that the X-ray emission of M87 nucleus may actually originate from the pc- or sub-pc-scale jet rather than the accretion disc. On the other hand, Di Matteo et al. (2003) argue that the observed radio-to-X-ray spectrum of M87 nucleus is consistent with that predicted by a radiatively-inefficient accretion disc. However, they can not also rule out the possibility that the X-ray emission of the nucleus is dominated by jet emission.

Considering this problem, it is also worthy to notice the latest research of Lenain et al. (2008). Similar to previous researches, Lenain et al. (2008) suggest that standard one-zone jet model can describe roughly the radio to X-ray SED of M87 nucleus (see also figure(1a) of Lenain et al. (2008)). They find, however, the single-zone approach cannot describe correctly the very high energy (VHE) emission of M87 detected by High Energy Stereoscopic System (HESS) telescope array. Their further research indicates that a multi-blob jet model of M87 nucleus may do better at TeV energy band. We note, however, there is some controversy on the origin of the unresolved TeV γ -ray source found in M87. For example, detailed modelling of Honda & Honda (2007) suggests that the VHE emissions may originate from bright knot A of M87 jet. Therefore, we argue that a single-zone approach of jet model is tolerable if our research interests focus only on radio to X-ray SED of M87 nucleus.

If the broad-band emissions of M87 nucleus mainly come from the unresolved compact jet region, it is necessary also to evaluate the influence of synchrotron-self-absorption effects at radio frequencies upon the result of synchrotron model fits. We find out that the radio spectrum of M87 nucleus is roughly consistent with a single power-law, i.e. $S_\nu \propto \nu^{-0.1}$. The flat radio spectrum implies that M87 nucleus is only partially opaque at the observed radio frequencies, and is far beyond the optically thick regime of synchrotron-self-absorption, i.e. $S_\nu \propto \nu^{2.5}$ (Pacholczyk 1970). Consequently, the synchrotron model fit to radio-to-X-ray SED neglecting the synchrotron-self-absorption effect should alter the derived break frequency only slightly, e.g. our derived $\nu_{\text{B,CI}} = 2.22 \times 10^{12}$ Hz is in good consistent with $\nu_{\text{B,CI}} = 2.8 \times 10^{12}$ Hz derived by Perlman et al. (2001b) based only upon mid-IR SED of M87 nucleus. We will further indicate that the deduced Doppler beaming factor is insensitive to the exact value of break frequency (see §3), therefore the simplification of broad-band fit to M87 nucleus at the radio frequencies should not alter the result significantly.

Inspection of Figure 1 and Figure 2 also indicates that there is systematic difference between CI and KP model fitting. KP model predicts higher break frequency than CI model does. Throughout M87 jet, CI model overpredicts the X-ray flux and the theoretical X-ray spectrum is flatter than that observed by *Chandra*. *Vice versa*, KP model underpredicts the X-ray flux, and the predicted X-ray spectrum is steeper than that observed. The same result is also achieved by Perlman & Wilson (2005). The systematic deviation of the two models off the X-ray spectra implies that the real position of ν_{B} may deviate also from standard CI and KP cases, or a modified non-standard synchrotron spectrum model should work better.

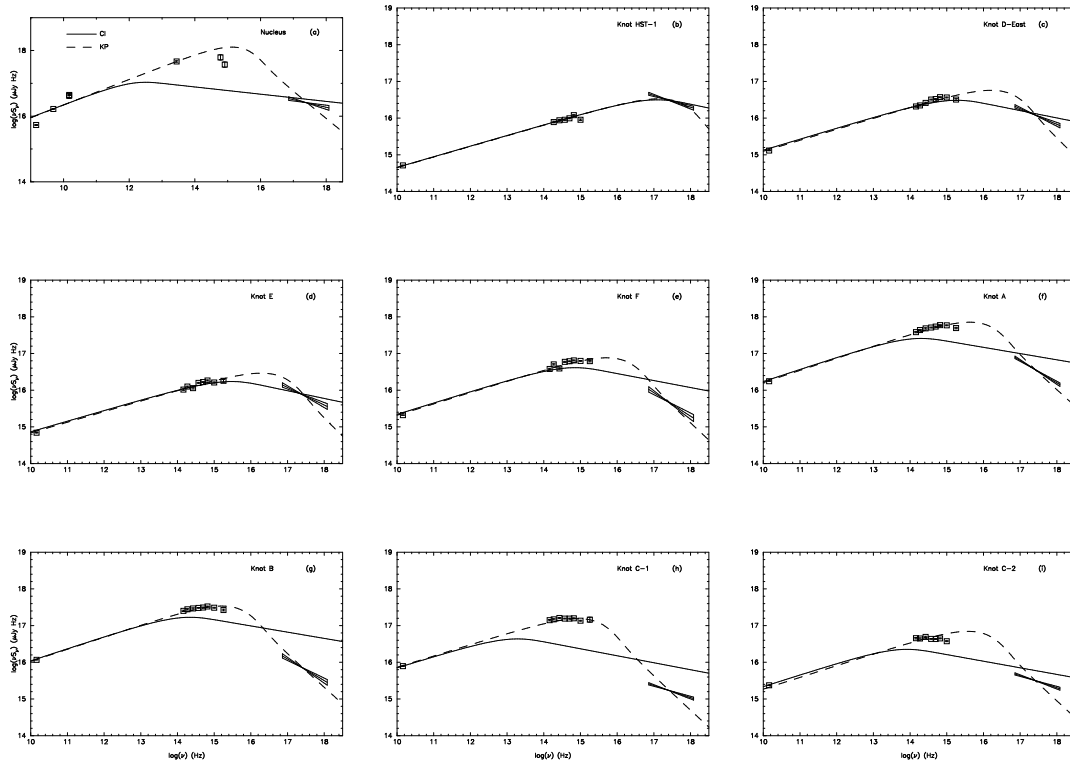


Figure 1. CI (solid line) and KP (dashed line) synchrotron spectrum model fits for nine regions along M87 jet. Data of knots are from: *VLA*-Zhou 1998; *HST*-Perlman et al. 2001a, Waters & Zepf 2005; *Chandra*-Perlman & Wilson 2005. Data of nucleus are from: *VLA*, *HST*-Sparks, Biretta & Macchetto 1996 and references therein; *Chandra*-Perlman & Wilson 2005.

Table 1. Best-Fit Parameters for Synchrotron Spectrum Models

Jet Region	α_{inj}	CI Model	KP Model
Nucleus	0.70	$\nu_B = 2.22 \pm 0.12 \times 10^{12} \text{ Hz}$ $\chi^2 = 119.47$	$3.29 \pm 0.07 \times 10^{15} \text{ Hz}$ 56.05
HST-1	0.71	$\nu_B = 1.84 \pm 0.09 \times 10^{17} \text{ Hz}$ $\chi^2 = 7.51$	$5.91 \pm 0.19 \times 10^{17} \text{ Hz}$ 5.69
D-East	0.70	$\nu_B = 2.58 \pm 0.10 \times 10^{15} \text{ Hz}$ $\chi^2 = 27.91$	$6.44 \pm 0.08 \times 10^{16} \text{ Hz}$ 36.30
E	0.71	$\nu_B = 4.36 \pm 0.22 \times 10^{15} \text{ Hz}$ $\chi^2 = 15.26$	$8.17 \pm 0.14 \times 10^{16} \text{ Hz}$ 20.83
F	0.69	$\nu_B = 8.95 \pm 0.43 \times 10^{14} \text{ Hz}$ $\chi^2 = 197.93$	$1.95 \pm 0.04 \times 10^{16} \text{ Hz}$ 14.41
A	0.67	$\nu_B = 2.16 \pm 0.06 \times 10^{14} \text{ Hz}$ $\chi^2 = 610.35$	$1.42 \pm 0.02 \times 10^{16} \text{ Hz}$ 18.81
B	0.67	$\nu_B = 2.38 \pm 0.07 \times 10^{14} \text{ Hz}$ $\chi^2 = 764.86$	$5.45 \pm 0.10 \times 10^{15} \text{ Hz}$ 8.58
C-1	0.69	$\nu_B = 2.42 \pm 0.06 \times 10^{13} \text{ Hz}$ $\chi^2 = 2554.64$	$3.30 \pm 0.04 \times 10^{15} \text{ Hz}$ 59.76
C-2	0.68	$\nu_B = 9.64 \pm 0.28 \times 10^{13} \text{ Hz}$ $\chi^2 = 508.73$	$1.34 \pm 0.01 \times 10^{16} \text{ Hz}$ 92.74

In order to explain such disagreement between the predicted and observed X-ray spectrum in M87 jet knots, several possible solutions to this problem are proposed. For example, if considering synchrotron cooling as well as electron acceleration processes in a non-uniform magnetic field, Bicknell & Begelman (1996) suggest it is possible to achieve a larger break in spectral index than standard CI model, i.e. $\Delta\alpha > 0.5$. With a similar scenario, Honda & Honda

(2007) obtain a modified X-ray spectral index consistent with *Chandra* observations of M87 knot A.

During the preparation of this paper, we also notice the latest result of Liu & Shen (2007). They propose a modified CI model to explain the radio-to-X-ray continua in six knots of M87 jet. Considering the thin acceleration region (i.e. shock front) locating at the immediately upstream of the main emission blob, the broadband spectra can be fit much better than standard CI model.

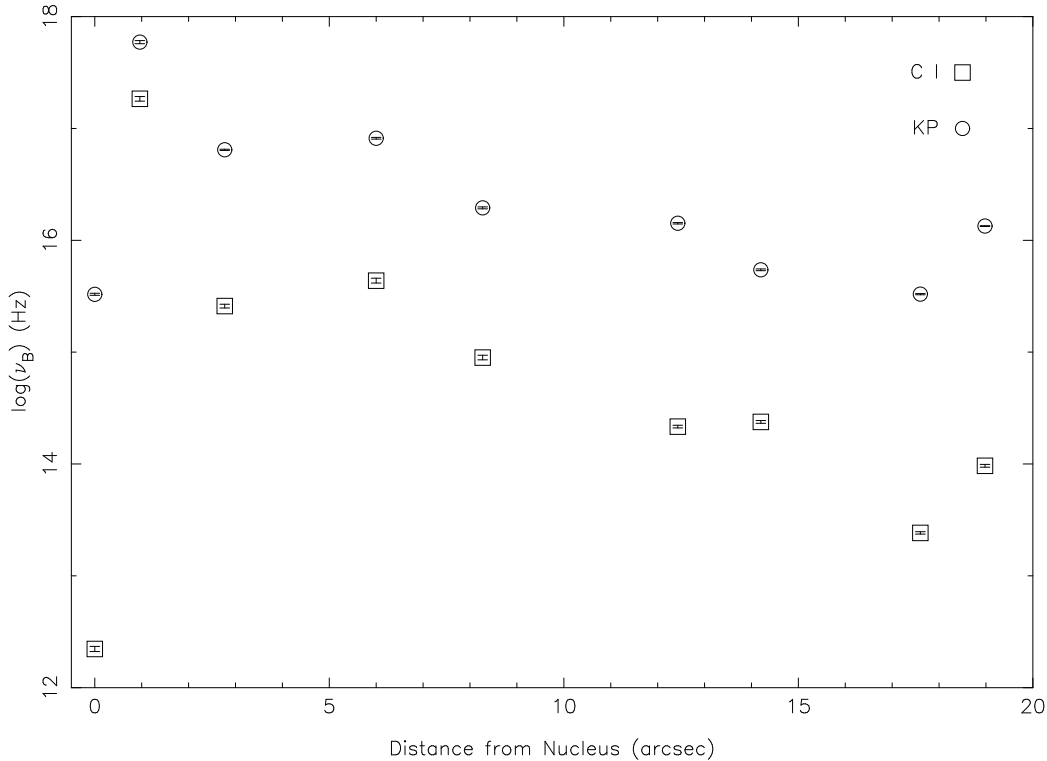


Figure 2. Derived break frequency through CI and KP model fitting versus the projected distance from jet nucleus.

3 DERIVING DOPPLER BEAMING FACTOR ALONG M87 JET

Through synchrotron spectrum model fitting, we can estimate break frequency (ν_B) of the observed SED. This frequency provides us with important information of the jet region. In general, we consider injection of a power-law distribution of relativistic electrons into an emission region dominated by synchrotron cooling process. Then the observed break frequency will correspond to a characteristic break energy of electron population ($\gamma = \gamma_{br}$), where synchrotron radiation loss is balanced by escape of electrons from the emission blob (e.g. Inoue & Takahara 1996, Kataoka et al. 2000).

Therefore we have an relation at the break frequency

$$t_{\text{syn}}(\nu_B) = t_{\text{esc}}, \quad (1)$$

where $t_{\text{syn}}(\nu_B)$ is synchrotron cooling time at the break frequency, t_{esc} is diffusive escape time scale of electrons from the emission region.

The synchrotron cooling time can be further expressed as

$$t_{\text{syn}}(\nu_B) = 5.08 \times 10^{16} B^{-3/2} \nu_B^{-1/2} \text{sec}, \quad (2)$$

where the magnetic field B , is in μG , and the break frequency ν_B , is in GHz.

Up to date, we know little about the random motion of electrons moving in the emission blob. Thus the escape time of electrons, t_{esc} , is quite uncertain. In general, it should be longer than light travel time over the source (R/c , where R is the size of the emission region and c is speed of light). The escape time, however, is unlikely to be much longer than R/c . Otherwise, no spectral break (ν_B) will be observed in

the SED, which is not the fact of the observations. We then adopt the treatment of Kataoka (1999) as

$$t_{\text{esc}} = \eta R/c, \quad (1 < \eta < 10) \quad (3)$$

where η is a dimensionless parameter. To estimate the influence of escape time upon the uncertainties of Doppler factor, we further assume that t_{esc} is Gaussian distributed in this regime (mean value $5.5R/c$, $\pm 3\sigma$ range), i.e. $\eta = 5.5 \pm 1.5$.

The equations above are all written in jet frame. Considering the relativistic bulk motion of the jet region described with a certain Doppler beaming factor, δ , there is a Lorentz transformation of the physical quantities from the source (jet) frame to the observer frame. According to the formulae presented in appendixes of Harris & Krawczynski (2002), Stawarz et al. (2003) and Begelman, Blandford & Rees (1984), we substitute (2) and (3) into (1) and rewrite the physical quantities in the observer frame. Thus Doppler beaming factor appears on both sides of the relation, which naturally leads to the final formula of δ (see Appendix A for details)

$$\delta = \left(\frac{\eta R_{\text{obs}}}{c} \times \frac{\nu_{B,\text{obs}}^{1/2} B(1)^{3/2}}{1.61 \times 10^{21}} \right)^{7/18}, \quad (4)$$

where R_{obs} is the mean observed radius of emission region in cm, c is speed of light in $\text{cm} \cdot \text{s}^{-1}$, $\nu_{B,\text{obs}}$ is the observed break frequency in Hz, $B(1)$ is the equipartition magnetic field in μG calculated for no beaming ($\delta = 1$). We compute $B(1)$ using eq. (A6) of Harris & Krawczynski (2002), which requires only total synchrotron luminosity and R_{obs} of the source. We can fit the radio-to-X-ray spectrum approximately with a single power law to estimate the observed bolometric luminosity of the jet region, following the treat-

ment of Harris et al. (2003). On the other hand, if we have FWHM measurement of the major axis (θ_a) and minor axis (θ_b) for a jet region from high resolution imaging observations, we can use the quantity $\sqrt{\theta_a \times \theta_b}$ to estimate the mean angular diameter of the region, which in turn gives R_{obs} with the known distance of the object. Due to the extreme proximity of M87 radio galaxy (distance = 16 Mpc), we neglect the redshift correction in equation (4), which requires an additional factor $(1+z)$ multiplied at the right side of that equation.

Although KP model gives better fits to broad-band spectra of M87 jet, this scenario is somewhat unrealistic. The spatial extent of the X-ray emitting regions in FR I jets resolved by *Chandra* implies that continuous acceleration/injection of high-energy electrons may occur in such objects. Therefore, the break frequency used in equation (4) to estimate Doppler factor should be derived from a more realistic modified CI model (e.g., Liu & Shen 2007). According to the definition of Liu & Shen (2007), their second break frequency, ν_{B2} , corresponds to the physical break frequency which relates to the break energy in the spectral energy distribution of relativistic electrons. They derive ν_{B2} for five knotty regions (D, F, A, B, C1), which agree with our $\nu_{B,KP}$ around a factor of 2. Furthermore, they also report the same decline of that break frequency down M87 jet.

On the other hand, we find in equation (4), $\delta \sim \nu_B^{1/5}$, which suggests the value of Doppler factor is insensitive to exact position of break frequency. Liu & Shen (2007) only give physical break frequency for five knots of M87 jet. To keep a standard treatment, we use $\nu_{B,KP}$ to approximate the physical break frequency derived from modified CI model in all nine regions along M87 jet.

We list in Table 2 the related parameters as well as derived Doppler factors for nine successive regions down M87 jet. Here R_{obs} is estimated using *Chandra* data of FWHM component sizes (see Table 1 of Perlman & Wilson 2005), for a scale of $1''=77.6$ pc. We notice that Kataoka & Stawarz (2005) calculate the equipartition magnetic field for three regions of M87 jet, i.e., knot HST-1, A and D. Their derived values of $B(1)$ which is based only upon chromatic radio luminosity, agree with our result within a factor of 2. Therefore our derived parameters are reliable.

The related parameters are substituted into (4), then the values of Doppler beaming factors are derived and listed in last column of Table 2. The uncertainties of δ are calculated using standard theory of error estimation. Our result provides strong support to the 'modest beaming' scenario (e.g., Harris et al. 2003) in this typical FR I radio galaxy. It is worthy to note the new result of Harris et al. (2006). They give the primary observational result of the long-term *Chandra* monitoring program of the variable knot HST-1. Harris et al. (2006) report the X-ray decay time of HST-1 for the intensity to drop by a factor of 2 range from 0.2 to 0.3 yr. Their detailed analysis suggests that small values of Doppler factor, i.e., $\delta \approx 3 - 5$, are favored for this knot. The result of Harris et al. (2006) is well consistent with our independent result for knot HST-1, i.e., $\delta \approx 3.06 - 4.08$. Moreover, Dodson, Edwards & Hirabayashi (2006) carry out detailed *VSOP* observations toward the nucleus region of M87 jet. Their study suggests that the M87 nucleus is not strongly Doppler boosted, with a Doppler beaming factor somewhat larger than 1.6. Our derived $\delta \approx 1.79 - 2.95$ for nucleus region

agree with their work again for this region. The consistency above then provides strong support to our new method.

4 DETERMINATION OF THE INTRINSIC VELOCITY FIELD AND DISCUSSIONS

Once δ and the observed apparent speed β_{app} of a jet region are available, we can compute the bulk Lorentz factor Γ and angle to line-of-sight θ using eq. (10) and (11) of Piner et al. (2003) as following:

$$\Gamma = \frac{\beta_{\text{app}}^2 + \delta^2 + 1}{2\delta} \quad (5)$$

and

$$\theta = \arctan \frac{2\beta_{\text{app}}}{\beta_{\text{app}}^2 + \delta^2 - 1}. \quad (6)$$

M87 owns detailed observations of proper motion for most of its jet knots. In Table 3, we list the observed data of apparent velocity β_{app} . Coupling the already derived Doppler factor δ , the bulk Lorentz factor and viewing angle of the knotty regions can be calculated with (5) and (6) (see also Table 3). The overall results are visualized in Figure 3.

First inspection of Table 3 indicates that the viewing angles of the inner jet regions are fully consistent with $10^\circ - 19^\circ$ to line-of-sight suggested by previous *HST* proper motions study of M87 jet (Biretta, Sparks & Macchetto 1999). For HST-1 knot, we use proper motion data up to $\sim 6c$, which are based on yearly *HST* optical monitoring from 1994 to 1998 (Biretta, Sparks & Macchetto 1999). Recently, Cheung et al. (2007) carry out VLBA monitoring of the same jet region from 2005 to 2006, and report apparent velocity up to $(4.3 \pm 0.7)c$, somewhat lower than previous *HST* measurement of Biretta, Sparks & Macchetto (1999). Combine this new apparent velocity with our derived Doppler factor of HST-1 knot, we find $\Gamma = 4.51 \pm 0.85$ and $\theta = 15.9 \pm 1.9$ deg. Our result agrees well with $\Gamma \geq 4.4$ suggested by Cheung et al. (2007). A comparison between two sets of results of HST-1 knot in two monitoring intervals suggests that the orientation of this jet region remains roughly the same, and the intrinsic velocity of jet flow suffers some decrease. Such a decrease of bulk velocity of the first knot of M87 jet may imply some reduced activity of its central engine.

As already noted by many researchers (e.g., Perlman et al. 2001a), the morphology of the outer M87 jet (knot A, B, C-1, C-2 in Table 3) is quite different from that of the inner jet (knot HST-1, D-East, E, F). Inspection of Table 3 and Figure 3 indicates that there is systematic difference on the intrinsic velocity as well as orientation between these two segment of jet flow. In Fig. (3b), we find the overall distribution of Doppler factor down M87 jet is quite flat, supporting the 'modest beaming' scenario. The inner jet, however, suffers sharp deceleration. On the other side, the intrinsic velocity of the bulk jet flow remains roughly constant in the outer jet (see Fig. (3c)). In fact, the similar general trend of β_{app} distribution (see Fig. (3a)) provides us with some hints.

In general, the early deceleration occurred in typical FR I jets such as M87 jet is believed to be caused by continuous mass loading through entrainment of ambient gaseous medium during jet propagation (e.g. Bicknell 1994). Based

Table 2. Related Quantities and Derived Doppler Factors Down M87 Jet

Jet Region	θ_a (arcsec)	θ_b (arcsec)	R_{obs} (pc)	$B(1)(\mu\text{G})$	δ
Nucleus	0.70 ± 0.04	0.58 ± 0.03	24.7 ± 1.0	699 ± 264	2.37 ± 0.58
HST-1	0.79 ± 0.06	0.60 ± 0.04	26.7 ± 1.4	237 ± 38	3.57 ± 0.51
D-East	0.85 ± 0.06	0.73 ± 0.05	30.6 ± 1.5	285 ± 121	2.72 ± 0.74
E	1.4 ± 0.2	0.9 ± 0.1	43.6 ± 3.9	183 ± 81	2.53 ± 0.71
F	1.6 ± 0.2	1.2 ± 0.2	53.8 ± 5.6	211 ± 143	2.26 ± 0.93
A	0.98 ± 0.04	0.91 ± 0.04	36.6 ± 1.1	547 ± 362	3.18 ± 1.27
B	1.7 ± 0.2	1.3 ± 0.2	57.7 ± 5.6	319 ± 250	2.30 ± 1.08
C-1	0.49 ± 0.00	0.49 ± 0.00	19.0 ± 0.0	871 ± 668	2.44 ± 1.12
C-2	0.49 ± 0.00	0.49 ± 0.00	19.0 ± 0.0	556 ± 355	2.46 ± 0.95

θ_a and θ_b are major and minor component sizes (FWHM), respectively, from *Chandra* observations (Perlman & Wilson 2005), R_{obs} is mean observed radius of emission region, $B(1)$ is equipartition magnetic field calculated for no beaming, i.e. Doppler beaming factor $\delta = 1$.

Table 3. Derived Intrinsic Velocity and Orientation of M87 Jet

Jet Region	β_{app}	Reference	Γ	θ (deg)
HST-1	6.14 ± 0.58	B99	7.21 ± 1.12	13.9 ± 1.2
D-East	2.99 ± 0.28	B99	3.19 ± 0.33	21.3 ± 5.1
E	3.92 ± 0.80	B99	4.50 ± 1.36	20.7 ± 3.8
F	0.86 ± 0.23	B95	1.51 ± 0.32	19.5 ± 16.0
A	0.5090 ± 0.0015	B95	1.79 ± 0.56	6.2 ± 5.3
B	0.62 ± 0.05	B95	1.45 ± 0.40	14.9 ± 15.1
C-1	0.11 ± 0.04	B95	1.43 ± 0.46	2.54 ± 2.94
C-2	0.11 ± 0.04	B95	1.44 ± 0.40	2.49 ± 2.46

β_{app} is observed apparent speed in unit c , Γ and θ refer to bulk Lorentz factor and viewing angle to line-of-sight of jet flow, respectively. References of proper motion observations are: B99 (Biretta, Sparks & Macchetto 1999), B95 (Biretta, Zhou & Owen 1995).

upon the derived velocity field here, we will explore the dynamics of deceleration of M87 jet deeply in a later paper (C. Wang et al., in preparation) that employs full treatment of special relativity hydrodynamics.

The orientation of inner jet and outer jet reveals different pattern also (see last column of Table 3 and Fig. (3d)). For the inner jet (knot HST-1, D-East, E, F), our derived viewing angles are fully consistent with 10° - 19° to line-of-sight suggested by the *HST* proper motion study of Biretta, Sparks & Macchetto (1999) in their Table 3. As to the outer jet (knot A, B, C-1, C-2), however, we find systematic deflection to much smaller viewing angles (Despite of the large uncertainties of viewing angle of knot B, we infer its most plausible orientation lies intermediately between that of knot A and knot C-1 considering smooth propagation of jet flow).

Lack of exact measurement of proper motion (e.g., Ly, Walker, & Junor (2007) give VLBI detected apparent speed of core jet as $(0.25 - 0.40)c$, while they argue it should be treated only as lower limits), we do not calculate the intrinsic velocity and orientation for the nucleus region of M87 jet. We argue, however, the viewing angle of M87 nucleus should be very close to the first knot, HST-1, i.e. $\theta \sim 15^\circ$ based upon mean estimation of values of $\theta \sim 14^\circ$ and 16° described above. Using the observed TeV band spectra of M87, Lenain et al. (2008) also constrain the orientation of its core jet as $\theta \sim 15^\circ$. Their results present good support

to our viewpoint. Therefore, the idea that M87 may be a misaligned blazar is favored by our research.

Here we explore further the somewhat strange orientation of the outer jet. We obtain small viewing angles ($\ll 10^\circ$) for the outer parts of M87 jet. The results conflict, however, with much larger inclination suggested by previous research (e.g., Bicknell & Begelman (1996) indicate the orientation of knots A and B should range between 30° - 40° to line-of-sight). From equation (4), we find Doppler factor is a slowly varying function of the magnetic field, i.e., $\delta \sim B(1)^{7/12}$. Then the uncomfortable small viewing angles of the outer jet may be the artifact of the assumed equipartition state of the magnetic field down the whole outflow. Moreover, we notice the research of Heinz & Begelman (1997) on M87 jet suggests that there is some departure from equipartition for the magnetic field of knot A, i.e., $0.2 < B/B_{\text{eq}} < 0.6$. Thus we can further evaluate the effect of magnetic field values on the derived jet orientation based upon their constraint to knot A.

With the constraint to knot A (Heinz & Begelman 1997), we assume the magnetic field of this jet region with no beaming, $B(1)$, has some departure from the related equipartition value (see column 5 of Table 2). Thus we have

$$B(1) = \xi B_{\text{eq}}(1), (0.2 < \xi < 0.6) \quad (7)$$

where ξ is a dimensionless parameter. Using different values of ξ , or different $B(1)$, we then repeat the same proce-

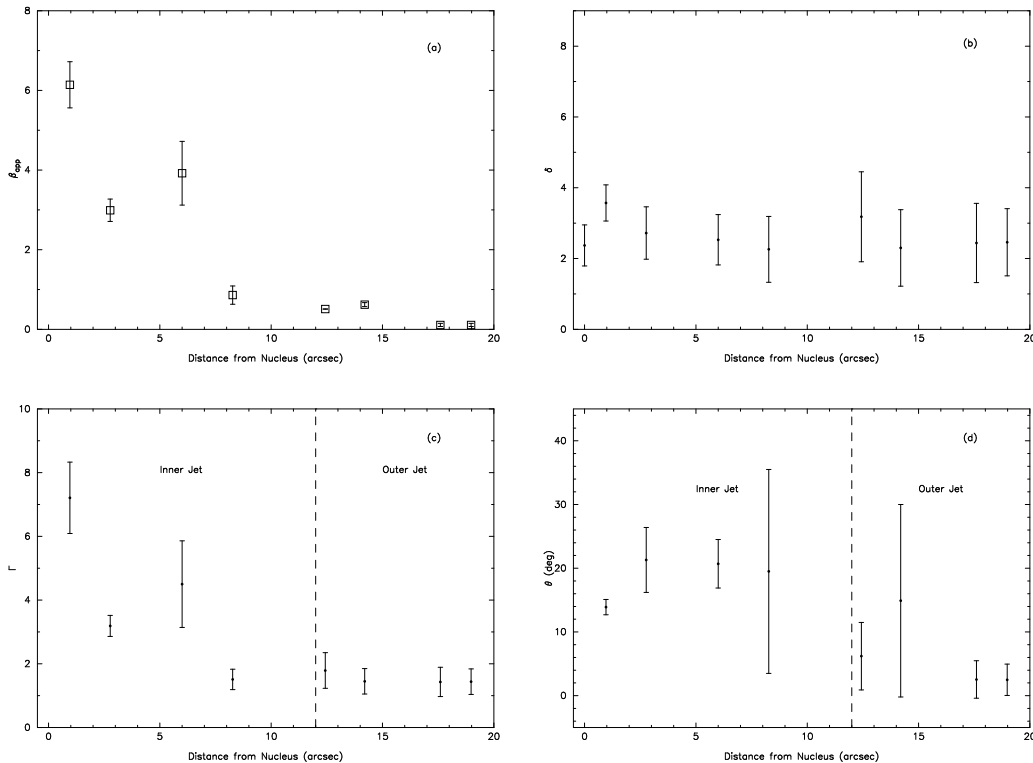


Figure 3. Plots of (a) observed apparent speed (in unit c), (b) Doppler beaming factor, (c) intrinsic bulk Lorentz factor and (d) viewing angle to line-of-sight versus projected distance down M87 jet.

dures described above to calculate the related Doppler factors, bulk Lorentz factors and viewing angles. The results are listed in Table 4.

Inspection of Table 4 suggests that the orientation of knot A depends on the level of departure from equipartition. If $0.4 < \xi < 0.6$ (small departure), its orientation can maintain the same viewing angle with the inner jet, i.e. $\theta \sim 10^\circ - 20^\circ$. Meanwhile, larger departure from equipartition ($0.25 < \xi < 0.3$) leads to large inclination ($\theta \sim 30^\circ - 40^\circ$) consistent with that inferred by Bicknell & Begelman (1996). Based on these results, we argue that the outer jet of M87 starting from knot A suffers some departure from equipartition. This departure may result from accumulative mass entrainment during jet propagation.

5 CONCLUSIONS AND SUMMARY

Based on multi-waveband fitting with moderate synchrotron spectrum models and radiation-escape balance at the break frequency, we derive the distribution of Doppler beaming factors down M87 jet. Coupling the data of proper motions, the intrinsic velocity and orientation are calculated for eight knotty regions, which presents some hints for the overall dynamics of this famous extragalactic jet. The main results are summarized as following:

- (1) The derived distribution of Doppler beaming factors gives good support to the 'modest beaming' scenario, with δ varying between $\sim 2 - 5$.
- (2) The bulk flow of M87 jet reveals sharp deceleration

at the inner jet, which may be caused by continuous entrainment of external gaseous medium during propagation. Meanwhile, the intrinsic speed of the outer jet remains roughly constant after early deceleration.

(3) The viewing angles of the inner jet regions are fully consistent with $10^\circ - 19^\circ$ to line-of-sight suggested by previous *HST* proper motions study of M87 jet. The outer jet, however, shows systematic deflection off the inner jet to much smaller inclination ($\theta \ll 10^\circ$). Further calculation of knot A suggests this deflection can be regarded as evidence that the outer jet suffers some departure from equipartition.

(4) The nucleus region of M87 jet should have an viewing angle close to its first knot HST-1, i.e. $\theta \sim 15^\circ$. Then our result favors the idea that M87 may be a misaligned blazar.

We should also comment the recent work of Laing & Bridle (2008). Using a relativistic jet model, Laing & Bridle (2008) try to model the high resolution VLA images of five FR I radio galaxies other than M87. They find that a decelerating jet model can fit the observed brightness and polarization structures well. Moreover, they suggest the deceleration is most likely caused by mass entrainment. Their results provide strong support to our result, i.e. the decelerating velocity profile found in typical FR I jet of M87 is reliable.

Once the related jet parameters are derived in Table (2) and Table (3), we can estimate the contribution to jet power carried by the radiating electrons and the magnetic field as (Kataoka et al. 2008)

$$L_j \approx 2\pi R^2 c \Gamma^2 \left(\frac{B'^2}{8\pi} \right), \quad (8)$$

Table 4. Kinetic Parameters of Knot A with Different Magnetic Field

ξ	δ	Γ	θ (deg)
0.25	1.42 ± 0.57	1.15 ± 0.11	38.6 ± 35.5
0.3	1.58 ± 0.63	1.19 ± 0.16	30.1 ± 28.2
0.4	1.87 ± 0.75	1.27 ± 0.24	20.3 ± 19.0
0.5	2.13 ± 0.85	1.36 ± 0.31	15.0 ± 13.7
0.6	2.36 ± 0.95	1.45 ± 0.37	11.9 ± 10.7

where the factor 2 means the total internal energy density is twice of the energy density of equipartition magnetic field. Making use of derived parameters of HST-1 knot and the transformation formulae in Appendix A, we get $L_j \approx 9 \times 10^{43} \text{erg.s}^{-1}$. Our result agrees well with $L_j \approx 10^{44} \text{erg.s}^{-1}$ suggested by different methods of previous researches (e.g., Bicknell & Begelman 1996, Stawarz et al. 2006).

Another issue we should confirm is whether our derived jet parameters are consistent with the conservation of the magnetic flux along M87 jet. In the jet frame, the magnetic flux $S = B'(\pi R'^2)$. Using derived jet parameters in Table (2) and transform with formulae of Appendix A, we can estimate the related magnetic fluxes (in $\mu\text{G.pc}^2$) as (the equipartition level of B in outer jet is somewhat uncertain, thus we only give results for inner jet regions): 7.23×10^5 (Nucleus), 2.14×10^5 (HST-1), 4.10×10^5 (D-east), 5.63×10^5 (E), and 1.07×10^6 (F). The results indicate the magnetic fluxes remain roughly conservative down the jet.

Finally, we should test the validity of main model assumption on the dominance of synchrotron cooling process. To compare the dominance of synchrotron cooling rate over SSC (synchrotron self-Compton) cooling rate, we have the ratio

$$\frac{(d\gamma/dt)_{\text{SSC}}}{(d\gamma/dt)_{\text{syn}}} = \frac{U'_{\text{ph}}}{U'_B}, \quad (9)$$

where $U'_B = B'^2/8\pi$ is the intrinsic energy density of magnetic field. The local energy density of photon field, U'_{ph} , can be estimated with intrinsic total synchrotron luminosity of the jet region, i.e. $U'_{\text{ph}} = L'_s/(4\pi R'^2 c)$. Making application to the jet parameters and observed total luminosity of jet regions, and transform with Appendix A, we find out the ratio defined in equation (9) range between $10^{-2} - 10^{-3}$ along M87 jet. The results are consistent with the model assumption on the dominance of synchrotron cooling.

Meanwhile, for the inner parts of the jet, the M87 host galaxy may provide relative intense photon field for the IC scattering process, resulting in an additional radiative cooling of the ultra-relativistic electrons. We should evaluate this possible effect in details. The star light from M87 host galaxy contributes to the jet as an incident external soft photon field at the optical band. To simplify the analysis, we assume the external photons have some characteristic frequency $\nu_{\text{ext}} \approx 5 \times 10^{14} \text{Hz}$. Then after external IC scattering (EC process) by ultra-relativistic electrons in the jet, the emerged high-energy photons will have some characteristic frequency as (Fossati 1998)

$$\nu_{\text{EC}} \simeq \frac{4}{3} \gamma^2 \delta \Gamma \nu_{\text{ext}}, \quad (10)$$

where γ is the Lorentz factor of the ultra-relativistic electron, δ and Γ refer to Doppler beaming factor and bulk Lorentz factor of the jet flow, respectively.

As to the ultra-relativistic electrons responsible for synchrotron X-ray emissions in large-scale jets, their typical energy should be $\gamma \sim 10^6$ or even higher. According to our inferred jet parameters of M87, we find $\delta \Gamma \sim 10$ for the inner jet regions. Therefore, the resulting high-energy photons from EC process locate around $\nu_{\text{EC}} \sim 10^{27} \text{Hz}$, which falls in the TeV energy band. The result above suggests that significant EC cooling of ultra-relativistic electrons from the host galaxy will predict significant contribution to the observed TeV spectra of M87. However, detailed study of Liu & Shen (2007) implies that the large-scale knots are unlikely to be the site for the TeV emissions recently detected in M87. Through modelling of the core jet of M87, Lenain et al. (2008) do not also find evidence of significant contribution to TeV emissions from EC process of M87 host galaxy. Therefore, we argue that the synchrotron cooling dominated assumption of the model should hold in the inner jet regions of M87.

During the preparation of this paper, we notice the latest work of Sahayanathan (2008) on M87 jet knots. An improved two-zone (emission region and nearby acceleration region) CI synchrotron model is presented by Sahayanathan (2008), very similar to the work of Liu & Shen (2007). Both of the modified CI models can fit the broad-band SED much better than standard synchrotron models for most of the M87 jet knots. We comment, however, another possibility for further improvement of the model. All of the current synchrotron models only consider synchrotron radiation of relativistic electrons spiralling in an uniform magnetic field, which is unlikely to be the real case.

It is generally believed that large-scale jet knots are places of strong shocks, where ultrarelativistic electrons are accelerated via the first-order Fermi process (e.g., Blandford & Eichler 1987; Ostrowski & Bednarz 2002). There is no strong evidence to support the suggestion that the magnetic field lines behind the shock front are straight and uniform. The structure of the magnetic field may be highly tangled, composed of curved magnetic field lines with different scales of radius.

On the other hand, theoretical researches on synchrotron radiation in curved magnetic field lines (Zhang & Cheng 1995, Cheng & Zhang 1996, Zhang & Yuan 1998; the mechanism is named 'synchro-curvature radiation' by the authors) suggest that the curvature of magnetic field lines plays an important role in the spectral slope of the synchrotron spectrum, i.e. at the high-energy portion of the SED. Recently, such a new mechanism was used to explain successfully the

high-energy excess of several gamma-ray bursts (GRBs; Deng, Xia & Liu 2005) the broad-band emission of which may also originate from relativistic jets. Since standard synchrotron models show systematic deviation from the observed X-ray spectra of M87 jet knots, it would be interesting also to explore the effect of curvature of magnetic field lines on the broad-band SED of the M87 jet and other objects in possible future work.

ACKNOWLEDGMENTS

We are grateful to Dr. E.S. Perlman for fruitful discussions and for supplying data of M87 jet as well as synchrotron model fitting code written by Dr. C. Carilli. The authors thank a lot the referee for very careful reading and valuable comments and suggestions. The authors also thank Dr. H.L. Marshall, Y.Y. Zhou, J.M. Bai and D.M. Meng for helpful discussions. C.C. Wang acknowledges Dr. J. Kataoka for continuous help on jet physics. This work is supported by Natural Science Foundation of China (NSFC) through grant NSFC 10673010 and NSFC 10473013. C.C. Wang acknowledges also support from Start-up Fund of USTC. This research has made use of NASA's Astrophysics Data System.

REFERENCES

- Begelman M.C., Blandford R.D., Rees M.J., 1984, *RvMP*, 56, 255
- Bicknell G.V., 1994, *ApJ*, 422, 542
- Bicknell G.V., Begelman M.C., 1996, *ApJ*, 467, 597
- Biretta J.A., Zhou F., Owen F.N., 1995, *ApJ*, 447, 582
- Biretta J.A., Sparks W.B., Macchetto F., 1999, *ApJ*, 520, 621
- Blandford R., Eichler D., 1987, *Phys. Rev.*, 154, 1
- Carilli C.L., Perley R.A., Dreher J.W., Leahy J.P., 1991, *ApJ*, 383, 554
- Casse F., Marcowith A., 2005, *Astroparticle Physics*, 23, 31
- Cheng K.S., Zhang J.L., 1996, *ApJ*, 463, 271
- Cheung C.C., Harris D.E., Stawarz L., 2007, *ApJ*, 663, L65
- Curtis H.D., 1918, *Lick Obs. Publ.*, 13, 31
- Deng X.L., Xia T.S., Liu J., 2005, *A&A*, 443, 747
- Di Matteo T., Allen S.W., Fabian A.C., Wilson A.S., Young A.J., 2003, *ApJ*, 582, 133
- Dodson R., Edwards P.G., Hirabaraishi H., 2006, *PASJ*, 58, 243
- Fossati G., 1998, PhD thesis, SISSA-ISAS
- Hardcastle M.J., Birkinshaw M., Worrall D.M., 2001, *MNRAS*, 326, 1499
- Harris D.E., Krawczynski H., 2002, *ApJ*, 565, 244
- Harris D.E., Biretta J.A., Junor W., Perlman E.S., Sparks W.B., Wilson A.S., 2003, *ApJ*, 586, L41
- Harris D.E., Cheung C.C., Biretta J.A., Sparks W.B., Junor W., Perlman E.S., Wilson A.S., 2006, *ApJ*, 640, 211
- Heavens A., Meisenheimer K., 1987, *MNRAS*, 225, 335
- Heinz S., Begelman M.C., 1997, *ApJ*, 490, 653
- Honda M., Honda Y.S., 2007, *ApJ*, 654, 885
- Inoue S., Takahara F., 1996, *ApJ*, 463, 555
- Jaffe W.J., Perola G.C., 1973, *A&A*, 26, 421
- Kardashev N.S., 1962, *Soviet Astron.-AJ*, 6, 317
- Kataoka J., 1999, Ph.D. Thesis, University of Tokyo
- Kataoka J., Takahashi T., Makino F., Inoue S., Madejski G.M., Tashiro M., Urry C.M., Kubo H., 2000, *ApJ*, 528, 243
- Kataoka J., Stawarz L., 2005, *ApJ*, 622, 797
- Kataoka J., Stawarz L., Harris D.E., Siemiginowska A., Ostrowski M., Swain M.R., Hardcastle M.J., Goodger J.L., Iwasawa K., Edwards P.G., 2008, *ApJ*, 685, 839
- Kraft R.P., Hardcastle M.J., Worrall D.M., Murray S.S., 2005, *ApJ*, 622, 149
- Laing R.A., Bridle A.H., 2008, *ASP Conference Series* 386 (Extragalactic Jets: Theory and Observation from Radio to Gamma Ray), T.A. Rector & D.S. Yong eds., 70, arXiv:0801.0147
- Leahy J.P., 1991, in *Beams and Jets in Astrophysics*, ed. P.A. Hughes (Cambridge: Cambridge Univ. Press), 100
- Lenain J.-P., Boisson C., Sol H., Katarzyński K., 2008, *A&A*, 478, 111
- Liu W., Shen Z., 2007, *ApJ*, 668, L23
- Lopez L.A., Brandt W.N., Vignali C., Schneider D.P., Chartas G., Garmire G.P., 2006, *AJ*, 131, 1914
- Ly C., Walker R.C., & Junor W., 2007, *ApJ*, 660, 200
- Marshall H.L., Miller B.P., Davis D.S., Perlman E.S., Wise M., Canizares C.R., Harris D.E., 2002, *ApJ*, 564, 683
- Meisenheimer K., Roeser H.-J., Hiltner P., Yates M.G., Longair M.S., Chini R., Perley R.A., 1989, *A&A*, 219, 63
- Myers S.T., Spangler S.R., 1985, *ApJ*, 291, 52
- Ostrowski M., Bednarz J., 2002, *A&A*, 394, 1141
- Pacholczyk A.G., 1970, *Radio Astrophysics* (San Francisco: Freeman)
- Perlman E.S., Wilson A., 2005, *ApJ*, 627, 140
- Perlman E.S., Biretta J.A., Zhou F., Sparks W.B., Macchetto F.D., 1999, *AJ*, 117, 2185
- Perlman E.S., Biretta J.A., Sparks W.B., Macchetto F.D., Leahy J.P., 2001a, *ApJ*, 551, 206
- Perlman E.S., Sparks W.B., Radomski J., Packham C., Fisher R.S., Pina R., Biretta J.A., 2001b, *ApJ*, 561, L51
- Piner B.G., Unwin S.C., Wehrle A.E., Zook A.C., Urry C.M., Gilmore D.M., 2003, *ApJ*, 588, 716
- Press W.H., Flannery B.P., Teukolsky S.A., Vetterling W.T., 1987, in *Numerical Recipes in FORTRAN* (Cambridge: Cambridge Univ. Press), 523
- Sahayanathan S., 2008, *MNRAS*, 388, L49
- Schwartz D.A., 2002, *ApJ*, 569, L23
- Sparks W.B., Biretta J.A., Macchetto F., 1996, *ApJ*, 473, 254
- Stawarz L., Sikora M., Ostrowski M., 2003, *ApJ*, 597, 186
- Stawarz L., Aharonian F., Kataoka J., Ostrowski M., Siemiginowska A., Sikora M., 2006, *MNRAS*, 370, 981
- Waters C.Z., Zepf S.E., 2005, *ApJ*, 624, 656
- Wilson A.S., Yang Y., 2002, *ApJ*, 568, 133
- Zhang J.L., Cheng K.S., 1995, *Physics Letters A*, 208, 47
- Zhang J.L., Yuan Y.F., 1998, *ApJ*, 493, 826
- Zhou F., 1998, Ph.D. thesis, New Mexico Inst. Mining & Technology, P99

APPENDIX A: RELATIVISTIC TRANSFORMATIONS TO DERIVE DOPPLER BEAMING FACTOR

In this section, we perform relativistic transformations from the jet rest frame (primed) to the observer frame (unprimed) to derive Doppler beaming factor of the jet knot. Firstly, let us assume that the jet knot, observed as a spherical emitting region with the radius R and the deprojected observed length $L \sim R$, is a moving blob.

In the jet rest frame, the synchrotron cooling time at the break frequency can be expressed as (Pacholczyk 1970)

$$t'_{\text{syn}}(\nu'_B) = 5.08 \times 10^{16} B'_{\text{eq}}{}^{-3/2} \nu'^{-1/2}_B \text{sec}, \quad (\text{A1})$$

where the equipartition magnetic field B'_{eq} , is in μG , and the break frequency ν'_B , is in GHz.

While performing Lorentz transformation from jet frame (primed) to the observer frame (unprimed), the break frequency transforms as (see formula (C6) of Begelman, Blandford & Rees 1984)

$$\nu'_B = \nu_{B,\text{obs}}/\delta. \quad (\text{A2})$$

Meanwhile, we use equation (A8) of Stawarz et al. (2003) to transform the equipartition value of the magnetic field, which corrects the formula (A7) of Harris & Krawczynski (2002). The transformation is expressed as

$$B'_{\text{eq}} = B(1)\delta^{-5/7}, \quad (\text{A3})$$

where $B(1)$ is the equipartition magnetic field calculated for no beaming ($\delta = 1$).

We then substitute equations (A2) and (A3) into (A1), and the synchrotron cooling time is rewritten as

$$t'_{\text{syn}} = 5.08 \times 10^{16} B(1)^{-3/2} \nu_{B,\text{obs}}^{-1/2} \delta^{11/7}. \quad (\text{A4})$$

On the other hand, in the jet rest frame, $L' = L/\delta \sim R/\delta$. Therefore we have the volume of the blob $V' = \pi R^2 L' = \pi R^2 L/\delta = V/\delta$. For the assumed geometry of the knot, the spatial scale of interest in the escape timescale is L' . Then we rewrite the form of escape timescale (Kataoka 1999) in the jet rest frame as

$$t'_{\text{esc}} = \eta L'/c, \quad (\text{A5})$$

where η is a dimensionless parameter, and c is speed of light in $\text{cm} \cdot \text{s}^{-1}$.

The relation above then gives

$$t'_{\text{esc}} = \eta \frac{L}{\delta c} \simeq \eta \frac{R}{\delta c}. \quad (\text{A6})$$

As to M87 jet, we have FWHM measurement of the major axis (θ_a) and minor axis (θ_b) for the jet knots from high resolution imaging observations by *Chandra* (Perlman & Wilson 2005). Therefore, we can use the quantity $\sqrt{\theta_a \times \theta_b}$ (in arcsec) to estimate the mean angular diameter of the region, which in turn gives average observed radius R_{obs} with the known distance of the object. The projection scale of M87 jet is $1'' = 77.6 \text{ pc}$, thus

$$R_{\text{obs}} = 0.5 \sqrt{\theta_a \times \theta_b} \times 77.6 \times 3.09 \times 10^{18} \text{cm}. \quad (\text{A7})$$

At the break frequency of the synchrotron spectrum, the synchrotron cooling time equals to the escape time of electrons from the main emission blob (e.g., Inoue & Takahara 1996, Kataoka et al. 2000). When we equal the right side of

equation (A4) and (A6), and rewrite $\nu_{B,\text{obs}}$ in Hz, the final formula of δ can be easily expressed as

$$\delta = \left(\frac{\eta R_{\text{obs}}}{c} \times \frac{\nu_{B,\text{obs}}^{1/2} B(1)^{3/2}}{1.61 \times 10^{21}} \right)^{7/18}. \quad (\text{A8})$$

This paper has been typeset from a $\text{T}_{\text{E}}\text{X}/\text{L}^{\text{A}}\text{T}_{\text{E}}\text{X}$ file prepared by the author.